QUANTUM SIMULATION AND NOISE ANALYSIS OF THE HEISENBERG SPIN CHAIN

Michael Rudnitsky-Ivan, Andrew Orndorff, Megan Reese, Benjamin Wingfield

In this project, we study how quantum systems can be simulated using quantum circuits under both idealized and realistic conditions. The work is organized into three phases that increase in complexity. First, we simulate the time evolution of a single qubit and compare circuit-based results with an analytic solution. Second, we study two-qubit dynamics using Trotter–Suzuki decompositions, allowing us to examine approximation error and the impact of circuit depth and noise. Finally, we apply the Variational Quantum Eigensolver (VQE) to estimate the ground-state energy of a small Heisenberg spin chain using ideal simulation, noisy simulation, and limited quantum hardware execution. Across these phases, we observe that shallow circuits can closely match theoretical predictions, while deeper circuits become more sensitive to noise and sampling effects. In the VQE experiments, increasing the ansatz depth improves the results in ideal simulations but does not lead to the same improvement when noise is included or when running on real hardware. Overall, the results illustrate the gap between ideal quantum algorithms and their practical implementation on current quantum devices.

1 Introduction

In this project, we study how quantum systems described by Hamiltonians can be simulated using quantum circuits under realistic constraints. While the mathematical formulation of quantum dynamics is well defined, implementing these models on current quantum hardware introduces several limitations. In particular, circuit execution is affected by noise, finite coherence times, and restrictions on circuit depth. As a result, it is important to understand how theoretical models are mapped onto executable circuits and how these constraints influence the observed behavior.

Rather than focusing on a single algorithm in isolation, this project approaches quantum simulation through a sequence of progressively more complex systems. Each stage introduces a new technical challenge that naturally arises in practice, including Hamiltonian decomposition, non-commuting operators, approximation error, and measurement noise. This structure allows us to build intuition incrementally while keeping the systems small enough to analyze and verify.

The project is organized into three phases. Phase 1 examines the time evolution of a single qubit under a general two-level Hamiltonian, where analytic solutions are available. This phase serves as a baseline for verifying that Hamiltonian dynamics are correctly implemented using quantum circuits. Phase 2 extends the system to two interacting qubits described by an Ising-type Hamiltonian. Because the Hamiltonian terms do not commute, time evolution must be approximated using Trotter–Suzuki decompositions, allowing us to study the tradeoff between approximation accuracy and circuit depth. Phase 3 shifts focus from time evolution to ground-state energy estimation using the Variational Quantum Eigensolver (VQE) applied to a small Heisenberg spin chain. [6, 7]

Across the three phases, ideal simulations are used as a reference for expected behavior. In Phases 2 and 3, noisy simulations are introduced to examine how approximation error and circuit depth interact with noise and finite sampling. In Phase 3, these results are further supplemented by limited execution on real quantum hardware. Together, these comparisons are used to evaluate how the simulated dynamics

and energy estimates change when subject to realistic experimental constraints. The goal is not to optimize performance, but to understand how Hamiltonian- based quantum simulations behave when implemented on currently available quantum devices. All code notebooks, formal theory notes, plot images, and this report are available in the public Github repository.

2 Background Theory

2.1 Single-Qubit Hamiltonians and Rabi Oscillations

The time evolution of a closed quantum system is governed by the time-dependent Schrödinger equation. [1] For a time-independent Hamiltonian H and using units where $\hbar = 1$, this equation takes the form

$$\frac{d}{dt}|\psi(t)\rangle = -iH|\psi(t)\rangle, \tag{1}$$

with the formal solution

$$|\psi(t)\rangle = e^{-iHt}|\psi(0)\rangle. \tag{2}$$

The operator $U(t) = e^{-iHt}$ is referred to as the time-evolution operator.

For a single qubit, any Hermitian Hamiltonian can be expressed as a linear combination of the identity and Pauli matrices,[1]

$$H = a_0 I + a_x \sigma_x + a_y \sigma_y + a_z \sigma_z, \tag{3}$$

where the coefficients are real. Assuming no imaginary components, the Hamiltonian may be written as

$$H = E_{\text{avg}} I + \Delta \sigma_z + \Omega \sigma_x. \tag{4}$$

The term proportional to the identity contributes only a global phase and does not affect measurement outcomes. The parameter Δ represents an energy offset between the computational basis states, while Ω sets the strength of the coupling that drives transitions between $|0\rangle$ and $|1\rangle$. Together, these parameters determine both the rate and amplitude of the resulting state evolution.

Because the identity operator commutes with all other terms, the time evolution separates as

$$e^{-iHt} = e^{-iE_{\text{avg}}t}\, e^{-i(\Delta\sigma_z + \Omega\sigma_x)t}. \tag{5}$$

Using the Pauli matrix exponential identity, this evolution corresponds to a rotation of the qubit state on the Bloch sphere about an axis defined by the relative contributions of the σ_x and σ_z terms.

To illustrate this behavior, we consider an initial state $|\psi(0)\rangle = |0\rangle$. The probability of measuring the qubit in the state $|1\rangle$ at time t is

$$P_1(t) = \frac{\Omega^2}{\Omega^2 + \Delta^2} \sin^2\!\left(\sqrt{\Omega^2 + \Delta^2}\, t\right). \tag{6}$$

This expression shows that the system undergoes a periodic transfer of population between the basis states. When $\Delta = 0$, the transition probability simplifies to

$$P_1(t) = \sin^2(\Omega t), \tag{7}$$

indicating complete population transfer between $|0\rangle$ and $|1\rangle$ over time.

This single-qubit model provides a simple and controlled setting for connecting Hamiltonian dynamics to quantum circuit implementations. By comparing the analytic predictions with circuit-based simulations, we can verify that the constructed circuits correctly reproduce the intended time evolution. This phase serves as a baseline for the more complex multi-qubit and approximate simulations explored in later sections.

2.2 Two-Qubit Interactions and Trotterization

To move beyond single-qubit dynamics, we next consider a system of two interacting qubits. The joint state of the system resides in the tensor product Hilbert space $\mathcal{H} = \mathbb{C}^2 \otimes \mathbb{C}^2$, with computational basis $\{|00\rangle, |01\rangle, |10\rangle, |11\rangle\}$. Operators acting on individual qubits are represented using tensor products of Pauli matrices and the identity.

In this phase, we study a two-qubit Ising-type Hamiltonian [4] of the form

$$H = J\,\sigma_{z_1}\sigma_{z_2} + \frac{\Omega}{2}\left(\sigma_{x_1} + \sigma_{x_2}\right), \tag{8}$$

where σ_{α_k} denotes the Pauli operator σ_α acting on qubit k, J is the coupling strength between the qubits, and Ω controls the strength of the local driving terms. The first term introduces an interaction that favors aligned or non-aligned spin configurations, while the local terms induce coherent single-qubit rotations.

It is convenient to decompose the Hamiltonian into commuting and non-commuting parts,

$$H = H_{ZZ} + H_{\text{local}}, \tag{9}$$

with

$$H_{ZZ} = J\,\sigma_{z_1}\sigma_{z_2}, \quad H_{\text{local}} = \frac{\Omega}{2}\left(\sigma_{x_1} + \sigma_{x_2}\right). \tag{10}$$

In contrast to the single-qubit case, these two components do not commute,

$$[H_{ZZ}, H_{\text{local}}] \neq 0, \tag{11}$$

which prevents the time-evolution operator from being written as a simple product of exponentials. As a result, the exact evolution operator $U(t) = e^{-i(H_{ZZ}+H_{\text{local}})t}$ must be approximated. [1]

A popular approach is the Trotter–Suzuki decomposition, which divides the total evolution time t into n smaller steps of size $\Delta t = t/n$ and alternates between evolutions generated by the individual Hamiltonian terms.

The first-order Trotter approximation [1, 5] is given by

$$e^{-i(H_{ZZ}+H_{\text{local}})t} \approx \left(e^{-iH_{\text{local}}\Delta t}e^{-iH_{ZZ}\Delta t}\right)^n. \tag{12}$$

As the number of Trotter steps n increases, the approximation error decreases, but the corresponding quantum circuit becomes deeper.

A more accurate approximation is provided by the second-order Trotter–Suzuki formula, [1, 5]

$$e^{-i(H_{ZZ}+H_{\text{local}})t} \approx \left(e^{-iH_{\text{local}}\Delta t/2}e^{-iH_{ZZ}\Delta t}e^{-iH_{\text{local}}\Delta t/2}\right)^n. \tag{13}$$

This second-order formulation reduces the Trotter approximation error for a fixed number of steps, but requires a slightly deeper circuit. The two-qubit system provides a controlled setting in which interactions and approximation error can be examined together. It allows us to directly compare exact evolution with Trotterized circuits and to observe how increasing circuit depth improves accuracy while also increasing exposure to noise.

2.3 Variational Quantum Eigensolver and Heisenberg Spin Chain

In the final phase of this project, we shift focus from time evolution to the estimation of ground-state energies using the Variational Quantum Eigensolver (VQE). Unlike direct Hamiltonian simulation, VQE is a hybrid quantum–classical algorithm that leverages parameterized quantum circuits and classical optimization to approximate the lowest-energy eigenstate of a Hamiltonian. [6, 7]

We consider the Heisenberg spin-chain Hamiltonian,[11]

$$H = J\sum_{\langle i,j\rangle}\left(\sigma_i^x\sigma_j^x + \sigma_i^y\sigma_j^y + \sigma_i^z\sigma_j^z\right), \tag{14}$$

where the sum runs over adjacent qubits in the chain and J sets the interaction strength. This Hamiltonian naturally decomposes into a sum of Pauli strings,

$$H = \sum_k h_k P_k, \tag{15}$$

with coefficients h_k and Pauli operators P_k acting on specific qubits. This decomposition is essential for VQE, as quantum hardware can efficiently measure expectation values of Pauli operators.

The variational principle states that for any normalized trial state $|\psi\rangle$,

$$\langle\psi|H|\psi\rangle \geq E_0, \tag{16}$$

where E_0 is the true ground-state energy of H. In VQE, this principle is used by preparing parameterized trial states,

$$|\psi(\boldsymbol{\theta})\rangle = U(\boldsymbol{\theta})|0\cdots0\rangle, \tag{17}$$

where $U(\boldsymbol{\theta})$ is a quantum circuit whose gate parameters $\boldsymbol{\theta}$ can be adjusted. A classical optimizer updates these parameters with the goal of lowering the measured energy,

$$E(\boldsymbol{\theta}) = \langle\psi(\boldsymbol{\theta})|H|\psi(\boldsymbol{\theta})\rangle = \sum_k h_k \langle P_k\rangle. \tag{18}$$

Each term $\langle P_k\rangle$ is estimated by repeatedly measuring the same circuit after applying the appropriate basis rotations. Terms involving only Z operators are measured directly in the computational basis, while X and Y terms require simple single-qubit rotations prior to measurement. Because these expectation values are estimated from a finite number of measurements, statistical fluctuations are unavoidable and can influence the optimization process, especially in the presence of noise. [6, 7]

The structure of the parameterized circuit determines the set of states that can be explored during the optimization. Circuits with fewer layers are simpler to implement but restrict the form of the trial state, while adding additional layers increases the number of adjustable parameters and circuit depth. These considerations make circuit depth an important design choice in VQE.

3 Methods

All simulations and experiments were performed using the Qiskit framework. [9] For each phase, we describe how the circuits were built, what parameters were chosen, and which values were used as references for comparison. Parameter choices were made to keep the systems small and interpretable, to limit circuit depth, and to make the effects of approximation and noise visible in the results.

3.1 Phase 1: Single-Qubit Rabi Oscillation

In Phase 1, we simulated the time evolution of a single qubit using a Hamiltonian with a known analytic solution. The detuning parameter was set to zero so that the expected population oscillations could be compared directly to the analytic $\sin^2(\Omega t)$ behavior. The overall energy offset was omitted since it does not affect measurement outcomes.

Time evolution was implemented using single-qubit rotation gates. The evolution time was varied uniformly over several oscillation periods so that the behavior could be clearly observed. Measurements were performed in the computational basis. In the noisy simulation case, probabilities were estimated by repeating the circuit multiple times.

3.2 Phase 2: Two-Qubit Ising Model Trotterization

In Phase 2, we studied a two-qubit Ising-type model containing both an interaction term and local field terms. The coupling strength was fixed to define the energy scale of the system. The local field strength was chosen to be of similar size so that neither part of the Hamiltonian dominated the evolution. This ensures that the effects of non-commutation are visible when approximating the dynamics.

Time evolution was approximated using first-order and second-order Trotter–Suzuki decompositions. The total evolution time was kept fixed while the number of Trotter steps was increased to study how the

approximation improves with circuit depth. Exact evolution obtained numerically was used as a reference. All circuits were evaluated using both ideal and noisy simulators to separate approximation error from the effects of noise.

3.3 Phase 3: VQE for a Four-Qubit Heisenberg Model

In Phase 3, we used the Variational Quantum Eigensolver to estimate the ground-state energy of a small Heisenberg spin chain. [8] The system size was chosen so that the exact ground-state energy could still be computed, allowing direct comparison with the VQE results.

Trial states were prepared using a hardware-efficient ansatz made up of parameterized single-qubit rotations and entangling gates between neighboring qubits. This ansatz was chosen to keep circuits relatively shallow while remaining compatible with available hardware. The number of ansatz layers was varied to study how increasing circuit depth affects the final energy estimate.

Energy expectation values were computed by measuring each Pauli term in the Hamiltonian using a finite number of shots. A gradient-free classical optimizer was used, since gradient-based methods are sensitive to noise and sampling error. Ideal simulations, noisy simulations, and limited hardware runs were performed where possible to study how noise, sampling variation, and circuit depth affect VQE performance.

4 Results

4.1 Phase 1: Single-Qubit Rabi Oscillation

The probability of finding the qubit in the $|1\rangle$ state follows the expected sinusoidal pattern of the analytic solution. Numerical simulation and qiskit simulation results match the analytic plot across the full evolution of time. Representative comparison plots are included in Appendix A.

4.2 Phase 2: Two-Qubit Ising Model Trotterization

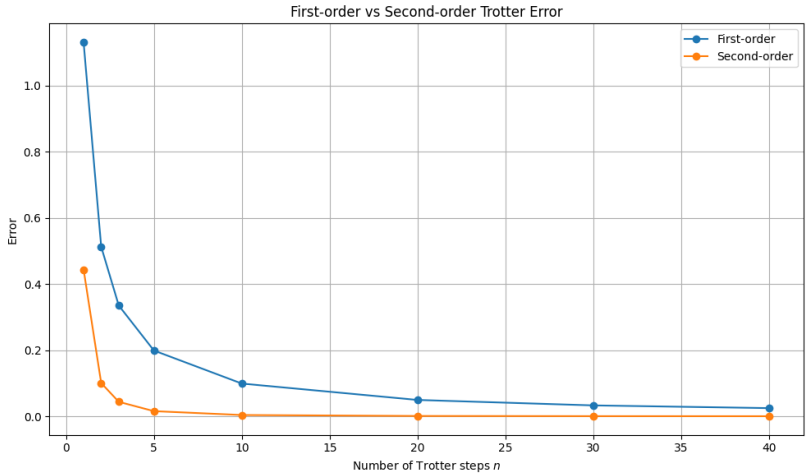

Fig. 1. Trotter approximation error as a function of the number of Trotter steps for first-order and second-order decompositions.

Figure 1 shows the Trotter approximation error as a function of the number of Trotter steps. For both first-order and second-order decompositions, the error decreases as the step count increases. For the step counts tested (up to $n = 40$), the second-order decomposition produces lower error than the first-order method.

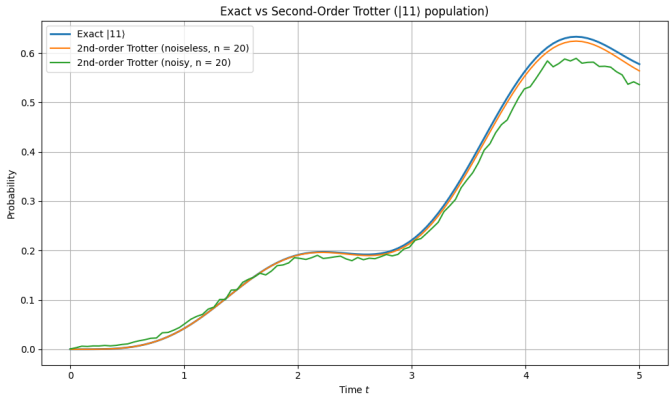

Fig. 2. Time evolution of the $|11\rangle$ population comparing exact evolution, noiseless second-order Trotterization, and noisy second-order Trotterization.

Figure 2 compares the time evolution of the $|11\rangle$ population obtained from exact evolution and second-order Trotterization. In the noiseless case, the Trotterized evolution closely tracks the exact result over the time interval shown. When noise is included, deviations from the exact evolution increase over time, with the largest differences appearing at later evolution times.

4.3 Phase 3: VQE for a Four-Qubit Heisenberg Model

The four-qubit Heisenberg Hamiltonian was diagonalized to obtain a reference ground-state energy of $E_{\text{exact}} = -6.4641$. This value is used as the comparison point for the VQE results below.

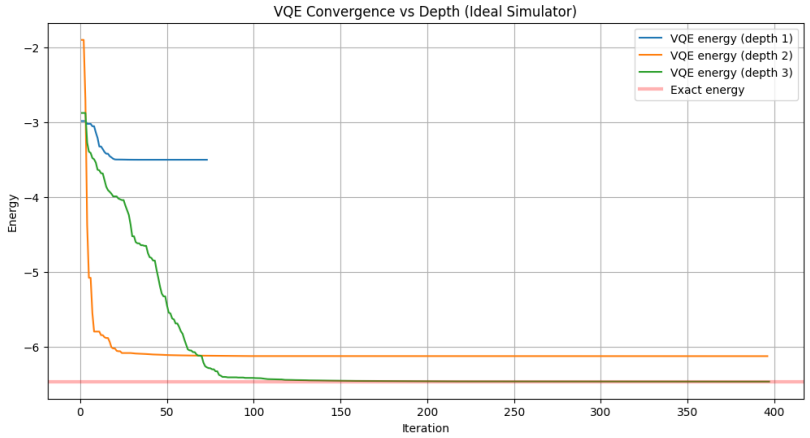

Fig. 3. Final VQE energies obtained for different ansatz depths using the ideal (noiseless) simulator. The exact ground-state energy is shown for reference.

Figure 3 shows the final energies obtained from noiseless VQE runs using ansatz depths of 1, 2, and 3. With a single layer, the VQE converges to an energy that is far from the exact ground state. Increasing the ansatz depth improves the final energy estimate. At depth 2, the final energy is within approximately 5% of the exact value, while at depth 3 achieves exact ground state value.

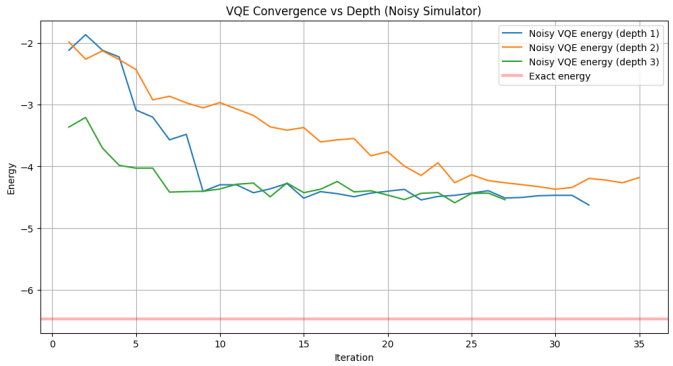

Fig. 4. Noisy VQE energy over optimization iterations for several ansatz depths.

Figure 4 shows the depth comparison under the noisy simulator. In contrast to the ideal case, increasing depth does not produce a clear improvement in the final energy. The final values vary across depths, and the noisy optimization traces show more fluctuation.

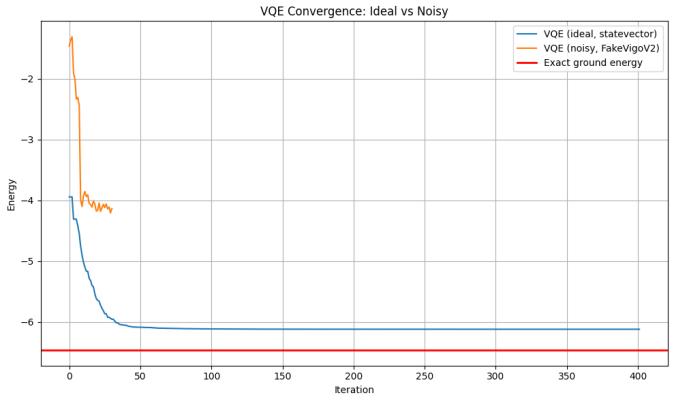

Fig. 5. VQE energy as a function of iteration number for ideal and noisy simulations at ansatz depth 2. The exact ground-state energy is shown for reference.

Figure 5 compares the behavior of ideal and noisy VQE runs at fixed ansatz depth 2. In the ideal case, the energy decreases smoothly over many iterations before leveling off near the final value. Under noisy simulation, the energy values fluctuate more from iteration to iteration and settle at a higher energy after a smaller number of iterations.

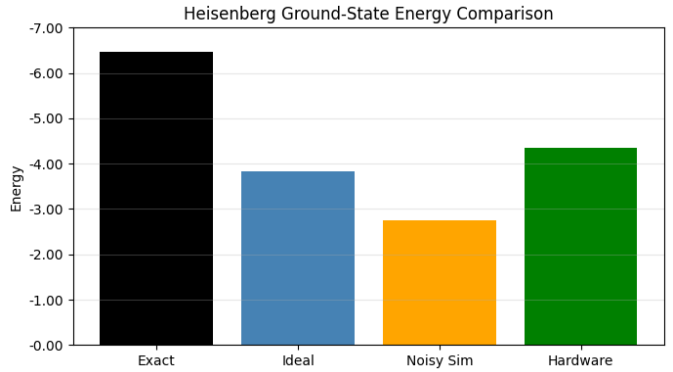

Fig. 6. Comparison of final energies obtained from exact diagonalization, ideal VQE, noisy VQE simulation, and hardware evaluation.

Figure 6 summarizes the final energies obtained from ideal simulation, noisy simulation, and hardware evaluation for ansatz depth 2. The ideal VQE result differs from the exact ground-state energy by approx-

imately 5.3%. The noisy simulation shows a much larger deviation. Evaluating the energy on quantum hardware at the noisy-VQE optimum yields an average value of -4.36, with a standard deviation of 0.08 across repeated measurements.

Additional plots and circuit diagrams are provided in the Appendix.

5 Discussion

The results from the experiments help to demonstrate the complications that need to be addressed when working with quantum systems and quantum hardware. For small systems, it is feasible to calculate the system analytically, but as the scale and complexity of the system increase, we must realistically resort to approximation methods, such as the Trotter decomposition demonstrated in this experiment. [1, 5] Moreover, quantum hardware introduces the constraint of using very simple gates, thus requiring mapping the system operator into a circuit of gates that the hardware can use. These complications highlight the emergence of error through the need for approximation and noise interference.

Phase 1 served as a primer for understanding fundamental concepts such as Hamiltonians, the Schrödinger equation, and how we can derive and apply these concepts so that we can work with and simulate quantum systems.

Phase 2 results start to show the emerging complications due to the rise in complexity of the system. In order to simulate the Ising model, we require a novel approach, which is given by Trotter decomposition. This method only provides an approximation, thus it is expected for some degree of error to be introduced. The results from Trotterization show that the accuracy of the approximation scales with the number of Trotter steps and inversely scales with time. Moreover, we observe how simulating noise amplifies the deviation in approximation accuracy. Additionally, the increase in error over time supports the assumed behavior of noise accumulation, which translates to increased inaccuracy.

Phase 3 results further highlight these issues by working with an even more complicated system. The VQE classical optimization procedure for approximating the ground-state energy contains errors by the nature of how optimizers function. This can be observed in our results by how the optimizer does not reach its maximum iteration limit on the noisy model, as it hits a local minimum that is far from the true ground-state energy level. Additionally, results show how increased depth of the ansatz circuit does not directly result in improved approximation and is exacerbated by noise interference. [7]

The hardware results showed unexpected outcomes by outputting a better approximation than the noiseless VQE approximation. Upon reflection, this is likely due to the low number of evaluations on hardware because of cost constraints and not sampling an average value for the noiseless and noisy VQE simulations. What these results do highlight is the variance in outcomes, which emphasizes the importance of careful planning when working with quantum systems and the challenges involved with current quantum hardware.

6 Conclusion

This project examined how quantum simulations behave when implemented using quantum circuits under both idealized and realistic noisy conditions. By moving from a single-qubit system to Trotterized two-qubit dynamics and finally to a variational algorithm for a small spin chain, we observed how approximation error, noise, and circuit depth increasingly affect performance as system complexity grows.

For simple systems and shallow circuits, simulated results closely match theoretical predictions. As circuits become deeper and noise is introduced, errors accumulate and limit the accuracy of both time evolution and energy estimates. While ideal simulations show that increased circuit expressiveness can significantly improve results, these improvements are harder to realize in noisy simulations and on real quantum hardware.

A natural next step would be to focus on optimizing algorithm hyperparameters, such as ansatz structure, circuit depth, shot counts, and optimizer settings. Better choices in these areas could lead to more accurate and more cost-effective simulations, particularly when hardware resources are limited.

References

1. M. A. Nielsen and I. L. Chuang, *Quantum Computation and Quantum Information*, 10th Anniversary Edition, Cambridge University Press (2010).
2. P. Kaye, R. Laflamme, and M. Mosca, *An Introduction to Quantum Computing*, Oxford University Press (2007).
3. T. G. Wong, *Introduction to Classical and Quantum Computing*, Rooted Grove (2022).
4. C. Külske, "The Ising model: highlights and perspectives," arXiv:2501.05394 (2025). doi:10.48550/arXiv.2501.05394.
5. C. Kluber, "Trotterization in Quantum Theory," arXiv:2310.13296v3 (2023). doi:10.48550/arXiv.2310.13296.
6. A. Peruzzo, J. McClean, P. Shadbolt, M.-H. Yung, X.-Q. Zhou, P. J. Love, A. Aspuru-Guzik, and J. L. O'Brien, "A variational eigenvalue solver on a quantum processor," *Nature Communications* **5**, 4213 (2014). doi:10.1038/ncomms5213.
7. J. Tilly, G. M. Graf, E. Endo, A. Fomin, M. Fujii, M. Hanks, A. Kosugi, S. Lee, J. Liu, A. Montanaro, S. Pattathil, and H. Yamamoto, "The Variational Quantum Eigensolver: a review of methods and best practices," *Physics Reports* **986**, 1–128 (2022). doi:10.1016/j.physrep.2022.08.003.
8. IBM Quantum, "Variational Quantum Eigensolver (VQE)," IBM Quantum Learning. Available: `https://quantum.cloud.ibm.com/learning/en/courses/quantum-diagonalization-algorithms/vqe` (Accessed: Fall 2025).
9. IBM Quantum, "Qiskit documentation guides," IBM Quantum Docs. Available: `https://quantum.cloud.ibm.com/docs/en/guides`.
10. S. Cantori, M. Pfaffhauser, F. Scafirimuto, and R. Davis, "Advancing quantum algorithms for large-scale simulations of quantum spin chains," IBM Quantum Blog (Oct. 30, 2024). Available: `https://www.ibm.com/quantum/blog/suny-stony-brook-spin-chain-simulations`.
11. S. Bhattacharya, V. B. Sabale, and A. Kumar, "Heisenberg spin chain models for realising quantum battery with the aid of Dzyaloshinskii–Moriya interaction," arXiv:2508.20529 (2025). doi:10.48550/arXiv.2508.20529.

Appendix A: Supplemental Figures

Phase 1: Single-Qubit Dynamics

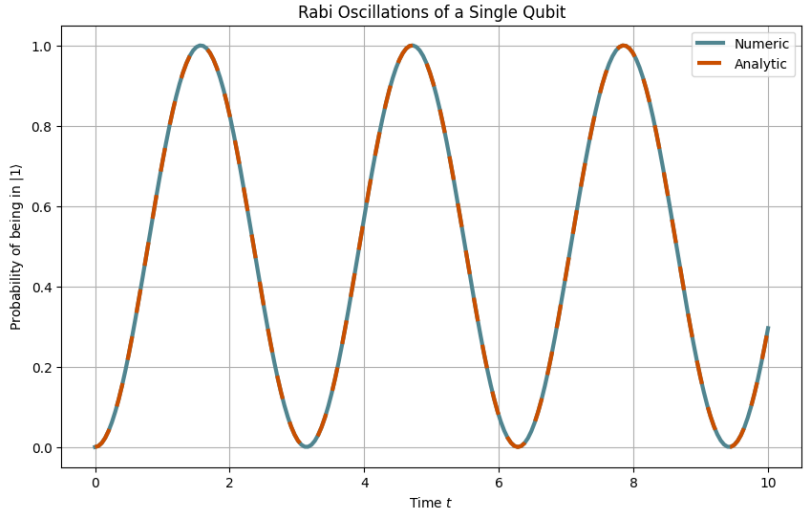

Fig. A.1. Single-qubit Rabi Oscillation dynamics from numerical results compared with the analytic result.

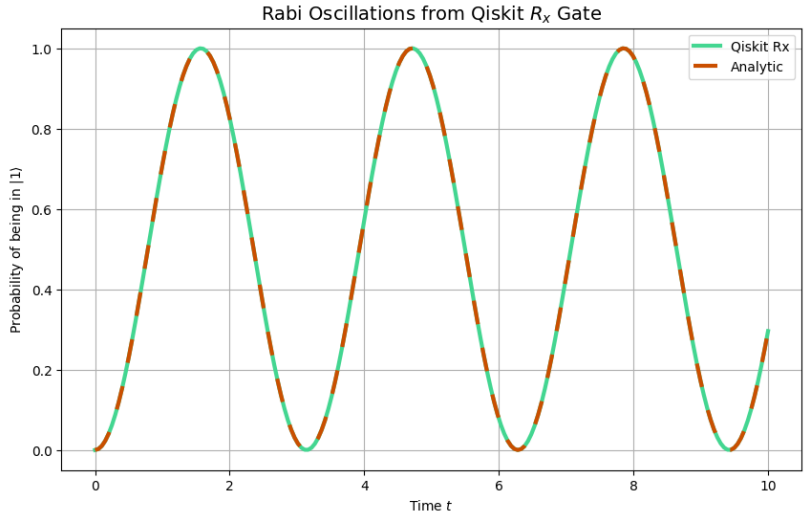

Fig. A.2. Rabi oscillations from circuit-based simulation compared with the analytic result.

Phase 2: Two-Qubit Trotterization

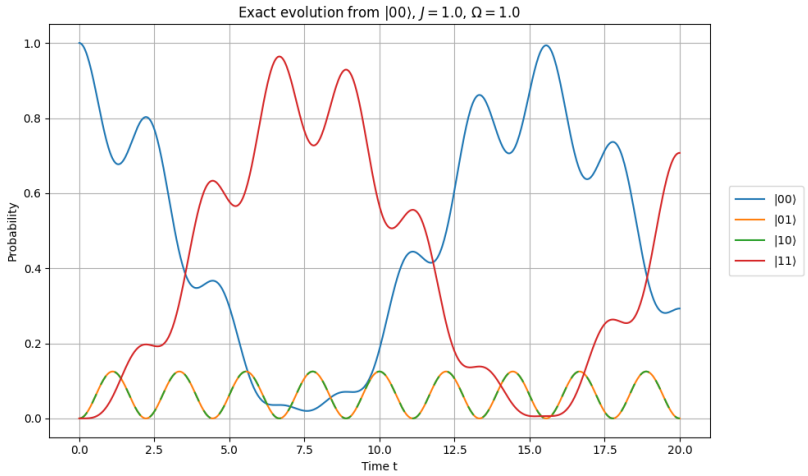

Fig. A.3. Exact two-qubit time evolution from the initial state $|00\rangle$ (all basis-state populations).

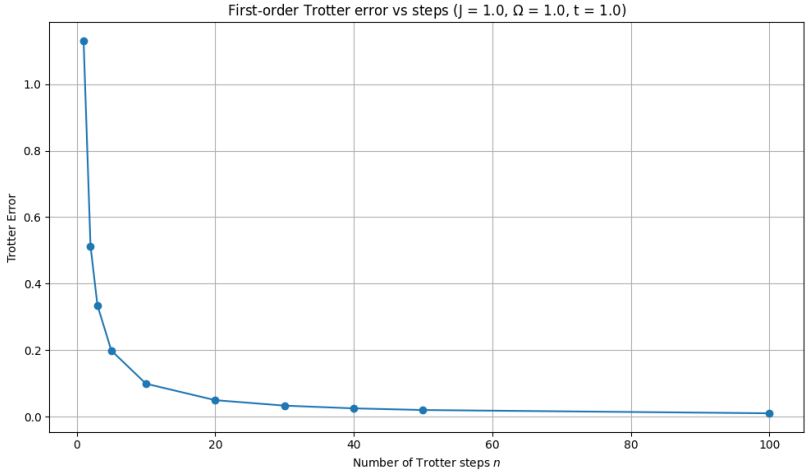

Fig. A.4. Error of first-order Trotterization as a function of the number of steps.

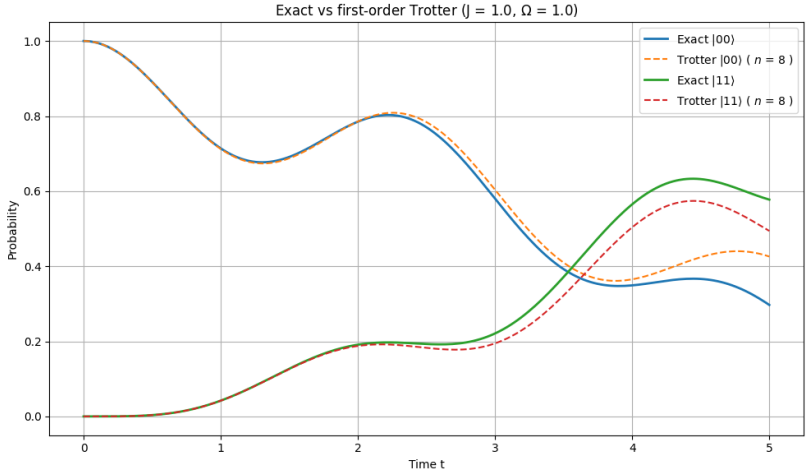

Fig. A.5. Comparison of exact and first-order Trotterization probability outcomes over time.

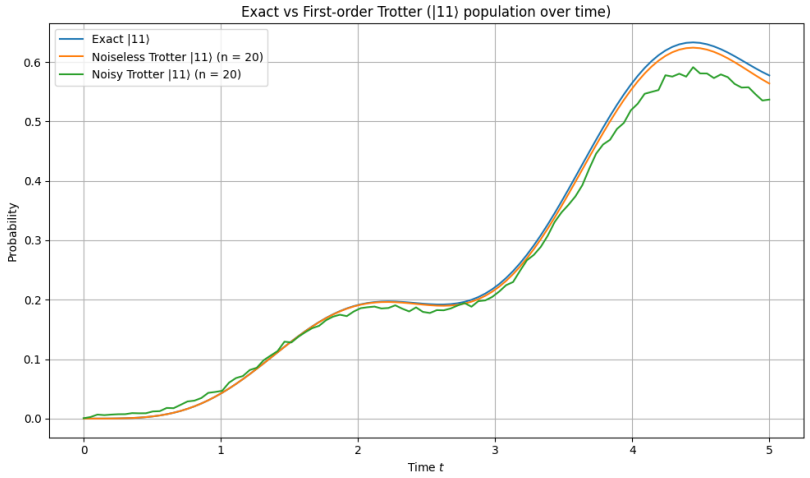

Fig. A.6. Deviation from exact probabilities for first-order Trotterization with and without noise.

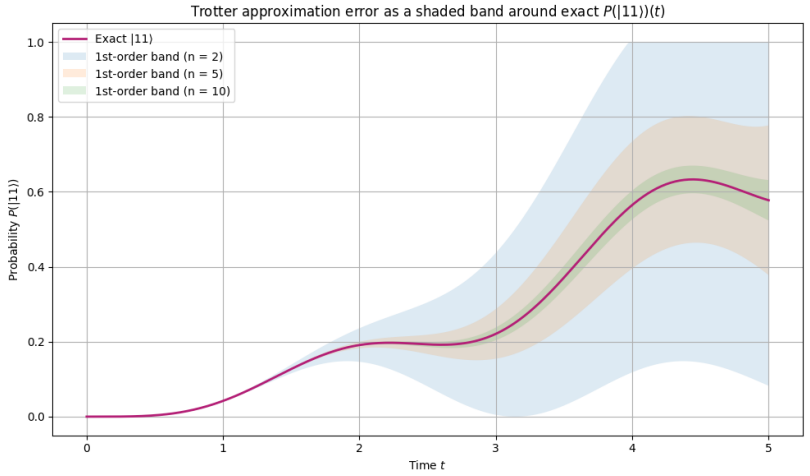

Fig. A.7. Effect of Trotter step count on approximation error shown as a band around the exact curve. *Note: band is used to signify the impact of error and not that the results are variable within the given band's range.*

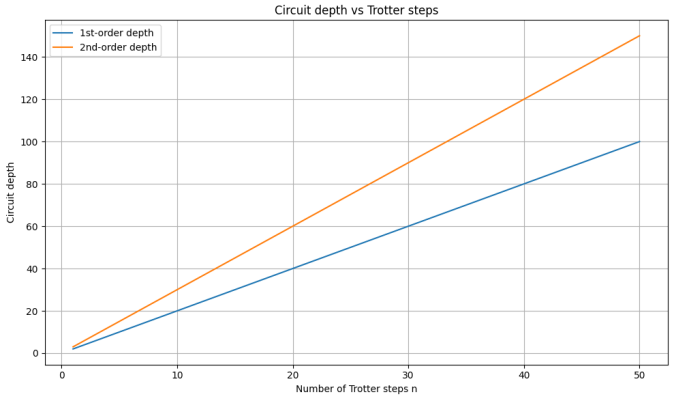

Fig. A.8. Circuit depth growth with Trotter step count for first-order and second-order decompositions.

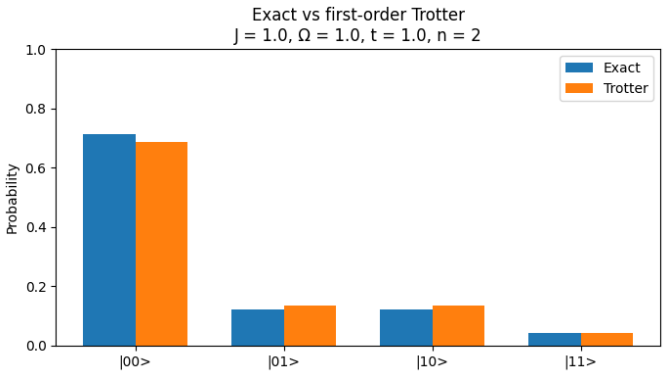

Fig. A.9. Population comparison at a fixed evolution time: exact vs first-order Trotterization.

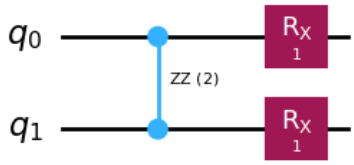

Fig. A.10. Circuit structure for a single step of first-order Trotterization.

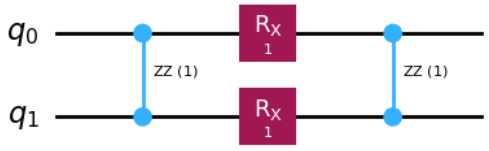

Fig. A.11. Circuit structure for a single step of second-order Trotterization.

Phase 3: VQE for the Heisenberg Model

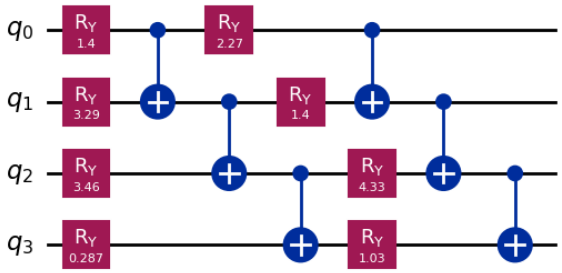

Fig. A.12. Example circuit diagram for VQE ansatz.

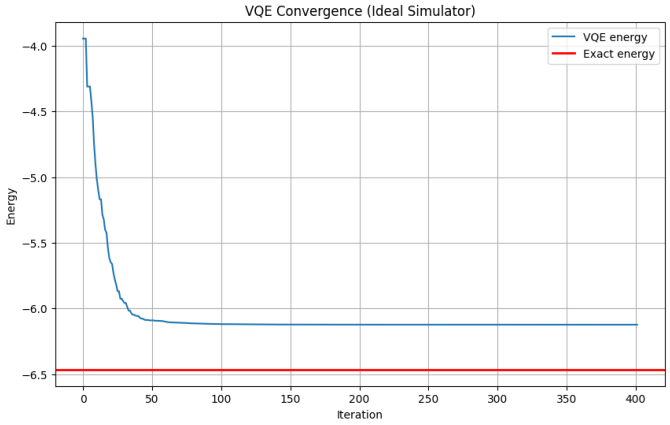

Fig. A.13. VQE convergence in the ideal simulator.

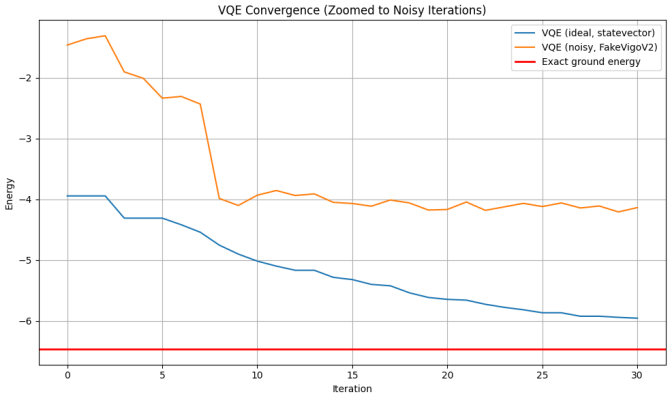

Fig. A.14. Zoomed view of the ideal VQE convergence curve.

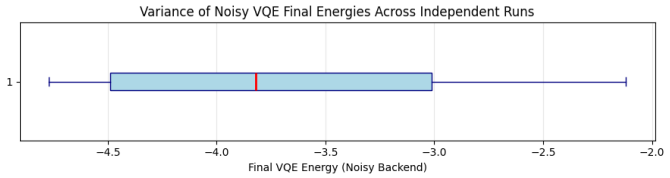

Fig. A.15. Variation of final energies across multiple independent noisy VQE runs.

Appendix B: AI Usage

AI tools were used throughout this project to help facilitate learning of the theory required for the experiments. Primarily helping to understand Hamiltonians and working on deriving how we identify and/or obtain them for our problem.

AI assistance was also used during the writing process to help edit grammar, improve sentence structure, and refine the overall flow of the report, with the exception of the Discussion section as specified by the professor's instructions. In addition, it was used to help translate handwritten or informally written mathematical expressions into proper LaTeX formatting.

During the implementation phase, AI tools were occasionally used to help debug code in the project notebooks and to resolve a small number of issues related to plotting and visualization using `matplotlib`. All experimental design choices, simulations, analysis, and interpretation of results were performed by the authors.